Dickson, C. L., Blundell, C. D., Butts, C. P., Felton, A., Jeffreys, A., & Takacs, Z. (2017). Accurate measurement of long range proton-carbon scalar coupling constants. *Analyst*, *142*(4), 621-633. https://doi.org/10.1039/c6an02298g

Journal Name

ARTICLE

Accurate measurement of long range proton-carbon scalar coupling constants

Received 00th January 20xx,
Accepted 00th January 20xx

DOI: 10.1039/x0xx00000x

www.rsc.org/

Claire L. Dickson,[a] Charles D. Blundell,[b] Craig P. Butts,[a†] Alice Felton,[a] Alex Jeffreys,[a] and Zoltan Takacs[b†]

The accuracy and practicality of measuring heteronuclear scalar coupling constants, $^{n}J_{CH}$, from modern NMR experimental methods is examined, based on F1 or F2 evolution of $^{n}J_{CH}$ in HSQMBC (including EXSIDE) and HMBC experiments. The results from these methods are compared to both robust experimental data (derived from coupled ^{13}C spectra), computed (Density Functional Theory) and literature values where available. We report on the accuracy, ease of use and time efficiency of these multi-dimensional methods and highlight their extent and limitations.

Introduction

New and more efficient NMR pulse sequences to measure multiple-bond heteronuclear ^{1}H-X (particularly ^{1}H-^{13}C) spin-spin scalar coupling constants, $^{n}J_{XH}$ (n>1), have been a feature of recent solution-state NMR methodology development. However there is little data reported on the accuracy and practical ease of using these approaches, leading to uncertainties about the reliability of these methods. On the other hand, multiple-bond scalar coupling constants capture valuable information regarding the geometry of the corresponding part of the molecule, for example $^{3}J_{XH}$ can be used to determine dihedral angles via Karplus equations.[1,2] These equations are well known for the homonuclear ^{1}H case but are less established for the heteronuclear case. This is unfortunate because of the information-rich potential of $^{n}J_{XH}$ couplings, in particular there are almost always many more heteronuclear ^{1}H-X couplings in a molecule than homonuclear ^{1}H-^{1}H couplings, and they can provide direct probes of the positions of non-protonated centres. The experimental methods to measure $^{n}J_{XH}$ have been reviewed,[3,4,5] but the focus has always been on the sensitivity, robustness and appearance of the spectra, rather than user-focussed issues such as accuracy of $^{n}J_{XH}$ values measured and ease of use of the techniques. It is these latter two, and specifically their application to ^{1}H-^{13}C couplings which are the focus of this report.[6]

In the case of homonuclear couplings, experimental values are usually readily determined from the 1D proton spectrum by just reading off the value from the splitting in the appropriate first order multiplet. Complexity in such analyses, arising from overlapping or second-order multiplets, can be addressed by data processing approaches, such as frequency/time-domain deconvolution and full density-matrix line-shape fitting, as well as experimental methods such as band-selective decoupling[7,8] or *J*-scaling[9]. Unfortunately, extracting heteronuclear $^{n}J_{XH}$ values from 1-dimensional spectra is very challenging due to low isotopic abundance, low gyromagnetic ratios and highly complex, often second-order, multiplets arising from coupling to abundant ^{1}H nuclei. While selectively-decoupled 1-dimensional heteronuclear spectra can reduce the latter of these problems in some cases, instead it is now routine to determine $^{n}J_{XH}$ coupling constants from heteronuclear inverse detected 2-dimensional NMR experiments. These 2-dimensional methods reduce spectrum overlap and in some cases can decrease the complexity of multiplets, but there are still numerous drawbacks to these - in particular around limitations in the means of magnetisation transfer and the need for extended refocussing periods, which in turn leads to low sensitivity. For example, magnetisation transfer by TOCSY mechanisms underpin a number of methods (HETLOC[10], HECADE[11], HSQC-TOCSY[12,13]) but are limited to measurement of couplings to protonated carbons. Given that the greatest value from heteronuclear couplings is often through insight into structure around quaternary carbons, this limitation can be severe. Further, many 2-dimensional methods do not present the $^{n}J_{XH}$ coupling constants in an easily readable form, instead the coupling must be extracted (usually by algorithmic fitting) from a complex multiplet.[14,15] The accuracy of the $^{n}J_{XH}$ coupling constants that can be extracted from such approaches is also uncertain and has not been compared to robust values derived from 1D heteronuclear spectra - although it should be noted that the precision of these experiments has been investigated before by Parella *et al*.[16,17] The 2-dimensional NMR methods are also often not amenable to non-expert use and there is a lack of practical

[a] University of Bristol, School of Chemistry, Cantocks Close, Bristol, BS8 1TS.
[b] C4X Discovery, Manchester One, 53 Portland Street, Manchester, M1 3LD, UK.
† to whom correspondence should be addressed
craig.butts@bristol.ac.uk
zoltan.takacs@c4xdiscovery.com
Electronic Supplementary Information (ESI) available. See DOI: 10.1039/x0xx00000x

understanding of their value for extracting couplings from 'real-world' molecules in 'real world' samples *i.e.* examples where fast relaxation or severe spectrum overlap must be considered. The increased complexity and requirement for evolution and refocussing delays in 2-dimensional NMR methods are often not well-suited for measurements of such 'real world' molecules. For example, when measuring ^{1}H-^{13}C coupling constants in the direct (horizontal) F2 dimension many approaches suffer from simultaneous evolution of ^{1}H-^{1}H and ^{1}H-^{13}C couplings with severe lineshape distortions arising from this. One way to address this it to eliminate ^{1}H-^{1}H coupling from the spectrum using HOBS/BASH[7,8] decoupling with no cost in sensitivity, however this necessitates measuring couplings to only one proton at a time (or a cluster of mutually uncoupled protons), which has a substantial time cost where a body of couplings are required. Castañar *et al* have reported the 'pure in-phase' (PIP) heteronuclear single-quantum multiple-bond correlation (HSQMBC) spectra,[18] which ensures clean ^{1}H-^{1}H and ^{1}H-^{13}C coupling co-evolution resulting in substantially improved F2 lineshapes but adding the ^{1}H-^{13}C coupling into already complex ^{1}H-^{1}H multiplets still makes it challenging to accurately measure coupling constants (especially those <2Hz) with this approach. The requirement for additional refocussing delays in these methods also imparts a sensitivity penalty, which can be severe for molecules experiencing relatively fast nuclear spin relaxation. Alternative approaches based on *J*-scaled sequences (EXSIDE[19], *J*-HMBC[20,21]) exploit very long INEPT transfer or evolution periods to separate the desired ^{1}H-^{13}C coupling in one or more frequency domains, and are correspondingly prone to sensitivity losses from relaxation, which can become catastrophic for measurements on some molecules. Given the variety of weaknesses and uncertainties when measuring $^{n}J_{CH}$ values, it is timely to provide clear evidence and guidelines for selecting and optimising experimental methods.

In this work we focus on accuracy and practicality of modern multi-dimensional NMR approaches to the measurement of accurate $^{n}J_{CH}$ coupling constants for model molecular systems, strychnine and camphor. The key criterion of this study is to examine methods that give reliably accurate (we are aiming for <0.5Hz accuracy) $^{n}J_{CH}$ values down to 1Hz, and measurement of couplings to both quaternary and protonated centres, through either evolution of the $^{n}J_{CH}$ in F2 (HMBC[32] and HSQMBC[16,32]) or *J*-scaled in F1 (EXSIDE). Crucially, we assess the accuracy of each method by comparison of control $^{n}J_{CH}$ values derived from 1-dimensional coupled ^{13}C spectra and consider issues of practicality (speed, sensitivity, ease of set-up and analysis) to propose selection guidelines for the various methods available. We do not assess methods which are aimed at extracting the sign of $^{n}J_{CH}$, for example selHSQMBC-TOCSY[22] or selHSQMBC-COSY[23], as despite the potentially crucial discrimination this provides for small $^{n}J_{CH}$ values, the accuracy of the sign measurement cannot be confirmed by the control (coupled ^{13}C) data. Case-specific methods that allow one to circumvent demanding molecule-specific limitations *e.g.* chemical exchange, substantial line broadening, or severe chemical shift overlap and generic modifications that have equal impact on all methods *e.g.* homonuclear decoupling (broadband *e.g.* PSYCHE[24] or Zangger-Sterk[25], or selective *e.g.* HOBS/BASH[7,8]), or non-uniform sampling,[26] are not explicitly examined, but their impact to circumvent these limitations are highlighted briefly as appropriate. The two molecules studied represent conservative model systems, with T1/T2 relaxation times in $CDCl_3$ (>0.4 seconds for strychnine and >2 seconds for camphor) that should not become limiting for multi-dimensional NMR methods.

Experimental

Compounds

All NMR samples were prepared as 30mg in 0.7ml of deuterated chloroform (strychnine 130mM, camphor 280mM) in 5mm tubes under air without degassing.

NMR Experiments

All spectra were recorded on a Bruker AVANCE III HD 500MHz NMR Spectrometer with 5mm DCH ^{13}C-^{1}H/D Cryo Probe or a Varian VNMRS 500MHz Direct Drive Spectrometer with Agilent OneNMR probe. The ^{1}H-coupled ^{13}C spectra were recorded with 3072 or 2048 scans and the selectively ^{1}H-decoupled spectra with 1172 or 1024 scans for strychnine and camphor respectively (Table S12). Selective ^{1}H-decoupling of certain ^{13}C spectra was achieved by using an MLEV-16 supercycle[27] combined with I2Snob shaped pulses[28].

For methods that evolve $^{n}J_{CH}$ in F2 512 to 1280 t1 increments were used in the indirect dimension with 4 to 12 scans each depending on sensitivity of the spectrum (Table S12). Adiabatic Chirp pulses were used in the zero quantum filter of 20-40ms length and a sweep frequency of 60kHz that was ~9.5 times higher than the spectral width in the proton dimension[29]. The spin state-selective IPAP HMBC[32], and refocused HSQMBC variants[18,32] were recorded in an interleaved fashioned (modified pulse sequences available in ESI), typically the odd experiments were chosen as in-phase (IP) and the even as antiphase (AP). Multiple coherence transfer times ($\Delta=1/(2\times J_{Long\ Range})$) in the INEPT periods were chosen (J_{LR}= 4, 6, 8Hz) to study effect on the accuracy and precision of the extracted coupling. The same approach was taken for the IP-only pure in-phase (PIP)-HSQMBC[18] spectra. For EXSIDE[19] which evolves $^{n}J_{CH}$ in F1 a wider range of coherence transfer times were tested (J_{LR}= 2, 4, 6, 8, 10Hz) with the number of t1 increments (Table S12) chosen to give an $^{n}J_{CH}$ resolution of 1Hz in the indirect dimension after scaling (N=30). For *J*-HMBC[20] J_{LR}=1Hz was used and the number of t1 increments chosen to give a scaling factor, κ, of 79 for strychnine and 56 for camphor across the respective spectral widths of 23873.5Hz and 28933.0Hz. A second-order low-pass filter was used ($^{1}J_{HC}$= 120Hz minimum to 175Hz maximum) to supress $^{1}J_{CH}$.

One-bond ^{1}H-^{13}C suppression was achieved in PIP-HSQMBC[18] by employing a TANGO excitation[30] following a GBIRD[31] in both the forward and reverse INEPT periods in the spectrum to be fitted and only in the forward INEPT period in the IPAP spectra. The refocused HSQMBC[32] spectra had a GBIRD type

suppression only in the forward INEPT period. The IPAP HMBC[32] spectra had a twofold low-pass filter for the same purpose. An accordion HSQMBC[33,34] was recorded by incrementing the Δ period in both the forward and backward INEPT from 62.5ms (~8Hz) to 166.67ms (~3Hz).

All spectra have been processed with NMRPipe[35] and/or MestReNova 9.0.1 NMR processing software. Direct dimensions were zero filled to 32k points and the indirect dimension twice. For the processing of IPAP spectra cosine-bell shaped apodization function was employed in both dimensions whereas the in-phase PIP-HSQMBC spectra subjected to line shape fitting had exponential line broadening with 0.2Hz in the direct dimension and cosine - bell shaped in the indirect dimension.

Spectrum Fitting Methodology

Spectral fitting was used to extract accurate couplings from 1D spectra (when first-order analysis was not possible) and 1D-slices (along F2) from 2D spectra. $^{n}J_{HH}$ were extracted from ^{1}H spectra and the resulting values were then used for fitting of the coupled ^{13}C or in certain slices of 2D spectra.

Spectral fitting has been described extensively in the past by various authors.[36] In this work, the calculations of transition frequencies and intensities from the density matrix of the spin system in question were carried out using the GAMMA software package[37]. The spectra were fitted using MINUIT2's[38] simplex algorithm[39] for regression and HESSE algorithm for error estimation. The HESSE errors reported represent a maximum range of error in $^{n}J_{CH}$ reflecting the peak linewidth and complexity. Where the fitting was found to be unstable, sensible starting parameters were identified from either a classical Lorentzian *a priori* analysis of simpler multiplets, or with a Monte Carlo analysis[40] for complex multiplets. The fitted $^{n}J_{CH}$ coupling constants were also constrained within physically realistic bounds (±30Hz) to help convergence of the fitting algorithms.

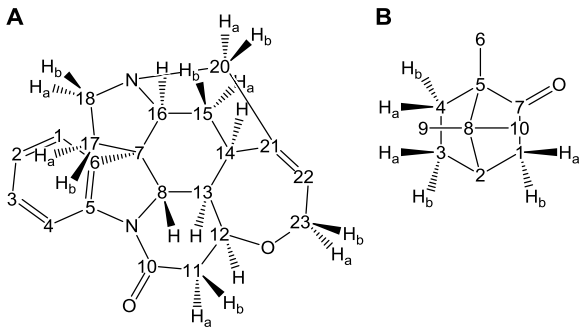

FIGURE 1. A) Strychnine, B) Camphor.

Computation of NMR Properties

Gaussian 09[41] was used to geometry optimise strychnine and camphor stepwise, first using molecular mechanics (MM) with the Uniform Force field (UFF), then using density functional theory (DFT) with B3LYP/3-21g, then mPW1PW91/6-31g (d,p) and finally mPW1PW91/6-311g (d,p). NMR calculations were performed with mPW1PW91/6-311g (d,p) using the GIAO method and including total scalar coupling constants, consisting of Fermi contact, paramagnetic spin orbit, diamagnetic spin orbit and spin dipolar terms. DFT calculations were performed using the IEFPCM (integral equation formalism polarizable continuum model) solvent model for chloroform.

Results and discussion

Coupled ^{13}C spectra

1-dimensional coupled ^{13}C spectra of strychnine and camphor (Figure 1) were used to establish a set of accurate 'gold-standard' $^{n}J_{CH}$ values. These spectra were collected with gated ^{1}H decoupling (*i.e.* decoupling on during relaxation delays and off during acquisition), therefore benefiting from NOE enhancement during the relaxation delay but allowing

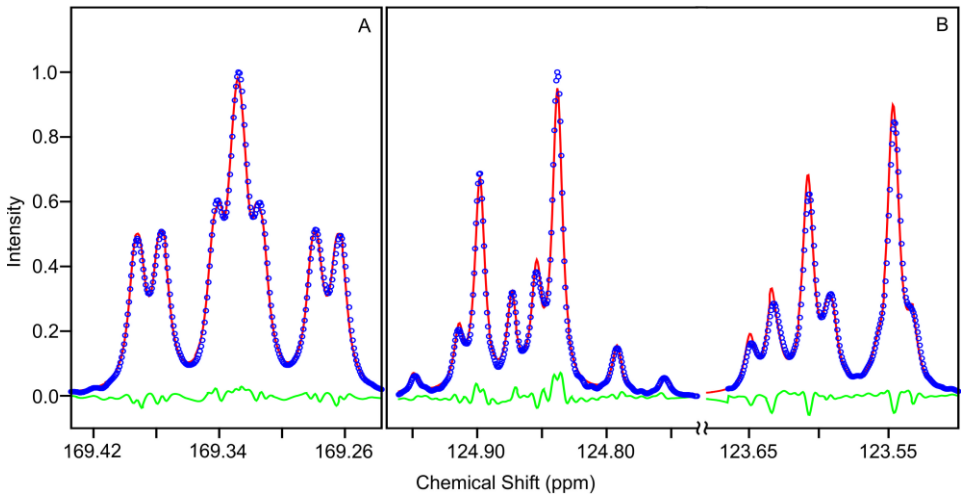

FIGURE 2. Coupled ^{13}C multiplets for A) C10 of strychnine B) C2 of strychnine; Blue circles represent the measured spectrum, the red line is the fitted spectrum and the green line is the absolute error.

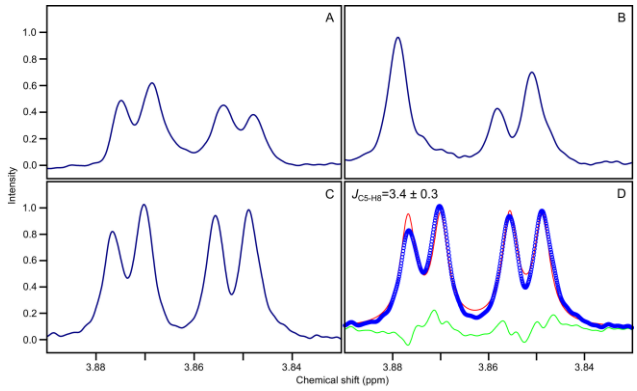

FIGURE 3. The C5 indirect slice of HSQMBC variants showing H8-C5 A) refocused HSQMBC J_{LR}=8Hz with no Zero Quantum filter B) PIP-HSQMBC J_{LR}=8Hz 20ms 60kHz Chirp pulse with 3% gradient C) PIP-HSQMBC J_{LR}=8Hz 40ms 60kHz Chirp pulse with 5% gradient D) fitting of C.

evolution of the ^{1}H-^{13}C coupling during the acquisition period. A comparison of the simple first-order ^{13}C multiplet arising from C10 of strychnine (Figure 2A) and the more complex second-order multiplet[42] for C2 (Figure 2B) demonstrates the challenge of extracting ^{1}H-^{13}C couplings from these 1-dimensional spectra.

Simulation and fitting procedures (see Methods section for details) were used to extract 55 gold-standard $^{n}J_{CH}$ values as possible from these spectra (Table S3B). Some $^{n}J_{CH}$ values could only be obtained by selectively decoupling ^{1}H resonances, in particular methyl groups in camphor, during acquisition to simplify multiplets. In order to simulate the relevant local spin systems for second-order spin systems such as Figure 2B, $^{n}J_{HH}$ values were extracted from 1-dimensional ^{1}H spectra (often by simulation as well, but this is a generally simpler process as each $^{n}J_{HH}$ coupling is present twice in the ^{1}H spectrum and ^{1}H-^{13}C coupling does not complicate multiplets). Where assignment of the simulated $^{n}J_{CH}$ coupling constants to particular ^{1}H-^{13}C pairs was ambiguous, this was achieved by comparison to values calculated using DFT with the best match between experimental and computed values being assumed to reflect correct assignments.

2D Methods that evolve $^{n}J_{CH}$ in F2

Almost all recently reported methods for measuring $^{n}J_{CH}$ couplings in the direct (F2) dimension of 2D NMR spectra are variants of three fundamental approaches, namely HMBC, refocussed and non-refocussed HSQMBC. Within these methods there are two broad approaches to analysing the ^{1}H-^{13}C coupling in the spectra, either lineshape analysis of F2 multiplets in the HMBC/HSQMBC spectra or IPAP analysis[43,44] of sum/difference spectra obtained from two separate in-phase (IP) and antiphase (AP) spectra. These two approaches to extracting $^{n}J_{CH}$ are based on similar underlying NMR sequences, but the relative merits of each technique for measuring *accurate* $^{n}J_{CH}$ values are worthy of comparison.

Lineshape analysis of HMBC/HSQMBC – Co-evolution of the ^{1}H-^{1}H and ^{1}H-^{13}C couplings during t2 of HMBC and HSQMBC spectra creates complex F2 multiplets from which the ^{1}H-^{13}C couplings must be extracted – but this very complexity makes accurate measurement of $^{n}J_{CH}$ directly from the multiplet difficult, and consequently for non-trivial molecules one must resort to lineshape fitting. Methods based on F2-evolution of $^{n}J_{CH}$ have been reported in a number of cases based on HMBC[15,20] non-refocussed HSQMBC[45,46] and pure in-phase HSQMBC (PIP-HSQMBC)[18]. The HMBC and non-refocussed HSQMBC methods are more sensitive than refocussed HSQMBC in cases where the protons in question relax fast but the lineshapes are substantially more complicated and the extraction of coupling constants is usually more challenging. Recently a F2-homonuclear decoupled PSYCHE HSQMBC[47] was reported to overcome the complexity of multiplets in these two cases however the severe loss in sensitivity of that experiment limits its value to only concentrated samples and so is not discussed in detail here.

In a refocused HSQMBC, the $^{n}J_{CH}$ coupling appears as an in-phase additional coupling in the proton multiplet. The key benefit to this technique is that the in-phase couplings can be manipulated to give cleaner lineshapes that are more easily fitted. Accurate extraction of the couplings from these multiplets still requires simulation and lineshape fitting in almost all cases (and thus require prior accurate measurement of all the contributing ^{1}H-^{1}H couplings) as well as a well-resolved multiplet. In order to make this simulation and extraction of $^{n}J_{CH}$ as easy as possible, ^{1}H-^{1}H *J*-modulation should be suppressed as it can perturb the peak shape. This is achieved with a Keeler-type Zero Quantum filter[29] at the end of the refocusing INEPT period and was reported as 'PIP-HSQMBC'[18]. These ZQ filters can require careful calibration of adiabatic pulses and gradients in order to obtain optimal lineshapes. Figure 3 illustrates the slightly distorted F2-lineshape obtained for the H8-C5 correlation of strychnine, without the ZQ filter (Figure 3A), which actually gets worse with poorly calibrated ZQ filter settings (Figure 3B), but is ultimately improved with optimised ZQ filter settings (Figure 3C). While none of the multiplets are without distortion, accurate fitting of essentially perfect Lorentzians is simply not possible for Figure 3B while the ZQ-filter optimised data in

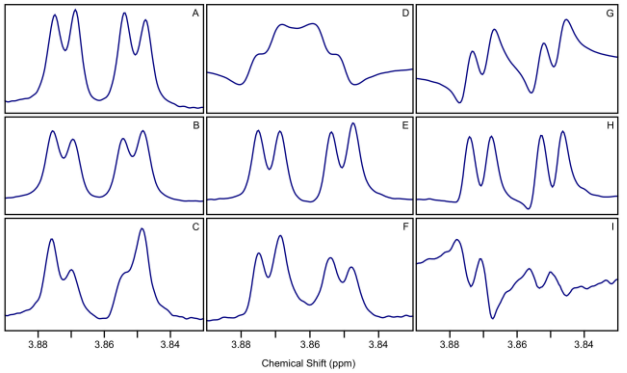

FIGURE 4. H8-C5 of strychnine ($^{n}J_{CH}$=3.2Hz) IP slices of PIP-HSQMBC, refocused HSQMBC and HMBC at different coherence transfer times A-C) PIP-HSQMBC with J_{LR}=4, 6, 8Hz respectively D-F) refocused HSQMBC with J_{LR}=4, 6, 8Hz respectively G-I) HMBC with J_{LR}=4, 6, 8Hz respectively; The PIP-HSQMBC spectra used a 20ms 60kHz CHIRP pulse and 3% in the ZQ filter.

Figure 3C can be at least reasonably fitted (shown in Figure 3D).

An alternative way to overcome the ^{1}H-^{1}H *J*-modulation is to use selective 180° ^{1}H pulses in the INEPT periods along with a so-called CLIP 90° ^{13}C pulse immediately before acquisition to convert the antiphase magnetization on ^{13}C to multiple quantum coherence[48]. This latter approach however limits the applicability of the sequence to protons that can be selectively excited, and also makes the experimental measurements much more time-consuming (see the EXSIDE discussion below for more on this point).

Figure 4 illustrates the substantial challenge of measuring $^{n}J_{CH}$ values using refocused HSQMBC without ZQ filters or simple HMBC methods.[32,16] The simple refocused HSQMBC (Figure 4D/E/F) and HMBC (Figure 4G/H/I) show lineshape variations for some values of J_{LR} which cannot readily be fitted while the PIP-HSQMBC gives reliably in-phase lineshapes for H8-C5 as a function of the evolution period (Δ/ J_{LR}) (Figure 4A/B/C),

Suppression of the 1-bond ^{1}H-^{13}C residual signals was achieved with TANGO excitation[30] and GBIRD[31] elements in both the initial and reverse INEPT periods. Of course the introduction of any extra elements such as the ZQ-filter, TANGO and/or BIRD further reduces the intensity of the faster relaxing peaks of these already long refocused HSQMBC sequences, but we found them very necessary in order to successfully fit the coupling constants from the complex multiplets generated by the refocused HSQMBC (reported in Table S3E). Throughout the manuscript we will refer to this sequence (including ZQ filter, TANGO and BIRD elements) as 'PIP-HSQMBC' and the sequence without these elements as 'refocused HSQMBC' for simplicity. In our hands the HMBC, non-refocussed and refocussed HSQMBC methods give data that are more challenging to fit reliably, hence we will only consider the fitting of PIP-HSQMBC further in this report.

IPAP HSQMBC – Another way HSQMBC and HMBC methods can be used to extract the *J*-couplings is to incorporate the spin state selective (in-phase antiphase, IPAP) principle, described by Parella *et al*.[16,48] In this type of experiment two separate datasets are recorded: one with the long range coupling in-phase (IP) and one with it antiphase (AP) with regard to ^{13}C.

The IP and AP experiments performed here were recorded interleaved, but can be recorded separately if desired. The sum and the difference of the two FIDs is formed in the time domain prior to Fourier transformation of each. An overlay of the sum and difference spectra then allows $^{n}J_{CH}$ to be extracted from the offset between multiplets in each spectrum, rather than from the splittings within the multiplets. This is shown in Figure 5. In principle, this makes it substantially easier to extract couplings because it does not rely on having resolvable lines within the multiplets nor on spectrum simulation and fitting procedures; however it does assume that the multiplet shapes of the sum and difference spectra are comparable, which is not always the case. The IPAP approach is much less sensitive than simple PIP-HSMQBC to ^{1}H *J*-modulation, since the modulation is the same in the two separate IP and AP experiments and thus has a consistent effect on both the sum/difference spectra and so does not affect the measured offset. There is therefore less benefit to incorporating a ZQ filter when using IPAP, unlike for lineshape analysis of the refocussed HSQMBC. Similarly, a ^{1}H-selective HSQMBC variant[49] gives improved lineshape over the original (non-PIP) HSQMBC methods, however the limitation to ^{1}H-selection is not necessary when applying IPAP because, *vide infra*, the broadband PIP-HSQMBC) gives sufficient quality of lineshape as it is also essentially phase insensitive because the only requirement is that the IP+AP should have the same phase as the IP-AP spectra.

This reduced sensitivity to lineshape distortion can be seen by comparison of the IPAP analysis of PIP-HSQMBC[18] (Figure 5A)

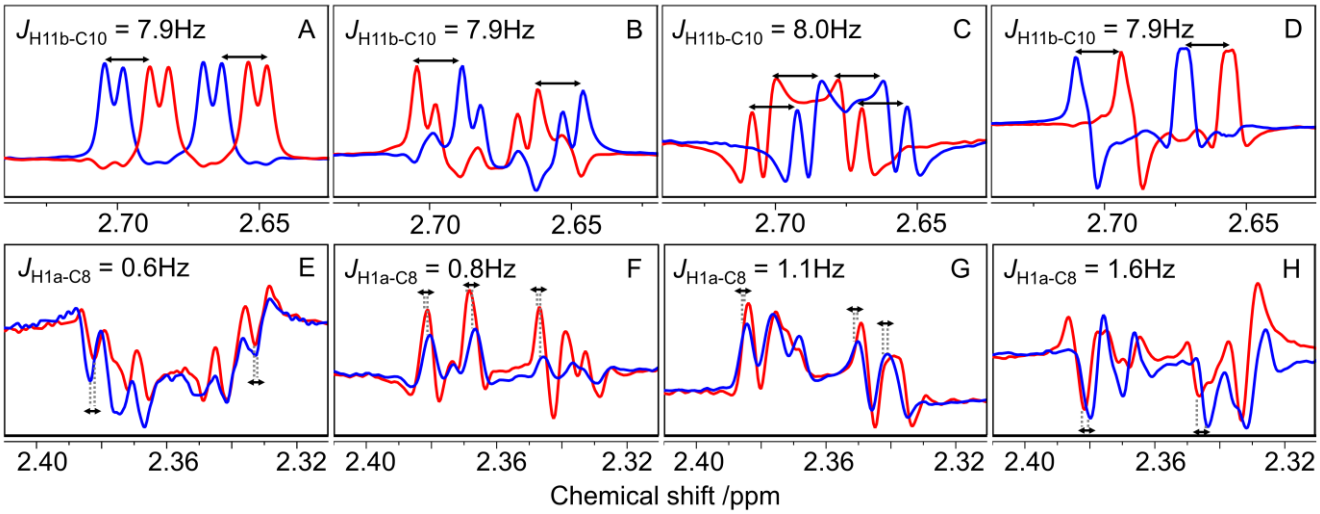

FIGURE 5. IPAP analysis of sum (red) and difference (blue) multiplets for H11b-C10 of strychnine using A) PIP-HSQMBC B) refocused HSQMBC C) Accordion-HSQMBC D) HMBC and H1a-C8 of camphor using E) PIP-HSQMBC F) refocused HSQMBC G) Accordion-HSQMBC H) HMBC. J_{LR} = 6Hz in all cases except the Accordion-HSQMBC where J_{LR} = 3-8Hz.

and refocused HSQMBC spectra (Figure 5B), where it is clear that the PIP-HSMQBC data has improved lineshape. While the refocused HSQMBC is still interpretable in principle (and gives a similar $^{n}J_{CH}$ if measured from the splitting between the main positive peaks) examination of the lineshapes reveals that the sum/difference lineshapes are not identical. An even starker example is provided by an Accordion[33,34] variant of the HSQMBC (Figure 5C) whereby very substantial lineshape distortion occurs, but because it arises equally in both sum and difference spectra the corresponding coupling constant can still be extracted. If major imbalances occur between the two datasets then the introduction of a post-acquisition scaling factor in the sum and difference step (IP±(k×AP)) can help to resolve this issue.[17] This does require that multiple sum/difference spectra are then generated in software in order to extract the maximum number of coupling constants, but does not require multiple experimental datasets to be acquired and so is relatively time-efficient.

It is useful to note that the measurement of small $^{n}J_{CH}$ values (<2Hz) is nearly always challenging due to insensitivity (so the multiplets are very weak) and substantial distortion of the multiplets from ^{1}H-^{1}H modulation. This latter point is clearly demonstrated in Figure 5E-H where all IP and AP datasets show severe distortion, however offsets between these sub-spectra can still provide reasonable estimates of their magnitudes in each case. A number of methods have been proposed to improve sensitivity to these small $^{n}J_{CH}$ values, such as HSQMBC/HMBC-COSY[32], which do provide increased numbers of correlations in this $^{n}J_{CH}$ range, particularly for the very smallest (<1Hz) couplings, *vide infra*.

IPAP HMBC – The IPAP analysis of HMBC32 operates in a very similar fashion to the IPAP analysis of HSQMBC data, so the couplings are measured from the offset of multiplets between sum and difference spectra obtained from combination of separately acquired IP and AP datasets. The $^{n}J_{CH}$ coupling constants extracted from analysis are presented in Table S3G. As described above, HMBC spectra give complex F2 lineshapes that are prone to phase distortion and *J*-modulation, making it difficult to extract accurate couplings from them directly. On the other hand, there is therefore a substantial benefit to be had from using the less phase and *J*-modulation sensitive IPAP approach to HMBC as shown in Figure 5D.

2D Methods that evolve $^{n}J_{CH}$ in F1

A different solution to the co-evolution of $^{n}J_{CH}$ and $^{n}J_{HH}$ is to allow the $^{n}J_{CH}$ coupling to evolve in the indirect (t1) evolution period while simultaneously refocussing the $^{n}J_{HH}$ couplings during this time. Generally this ^{1}H-^{1}H decoupling is achieved by using selective ^{1}H inversion of the active spin(s) (the ^{1}H nuclei for which the user wishes to measure $^{n}J_{CH}$) and is thus limited to only ^{1}H resonances that can be selectively excited without simultaneously exciting one of their coupling partners. The resulting F1 doublets encode the $^{n}J_{CH}$ coupling constant and are extremely simple to interpret, making these very desirable methods for non-expert users. However, to resolve the small $^{n}J_{CH}$ couplings in F1 one must measure exceedingly high

TABLE 1. Summary of $^{n}J_{CH}$ values measured in this study

	DFT[b]	Coupled ^{13}C[c]	IPAP accordion HSQMBC	IPAP PIP-HSQMBC	IPAP HMBC	IPAP refocussed HSQMBC	EXSIDE[d]	*J*-HMBC	PIP-HSQMBC[f]	Lit.[h]
No. of $^{n}J_{CH}$	143	55	96	74	89	74	73	98	20	47
% of 143 $^{n}J_{CH}$ measured		38	67	52	62	52	51	69	19	33
MAD (SD) /Hz[a]	0.38 (0.49)		0.33 (0.45)	0.22 (0.34)	0.35 (0.40)	0.33 (0.52)	0.14 (0.19)	0.28 (0.44)[e]	0.18 (0.14)[g]	0.62 (0.84)
Exp. time per $^{n}J_{CH}$ /min		30	3	7	6	6	41	2	14	
Range of analysis time per $^{n}J_{CH}$ /min		Up to 72 hours	1-20	1-20	1-20	1-20	1-3	1-10	15-25	

[a] Mean absolute deviation/standard deviation (MAD/SD) calculated by comparison to coupled ^{13}C values.

[b] $^{n}J_{CH}$ >1Hz calculated by DFT with a 6% linear correction applied as per discussion in main text.

[c] The reported values were taken from full matrix spin simulations and fitting of coupled ^{13}C spectra by preference. Where these line shapes could not be simulated effectively due to the complexity of the lineshapes, the values are reported from simulation and fitting of selectively decoupled ^{13}C spectra.

[d] MAD/SD calculated from 'tilted' EXSIDE values. See main text for details.

[e] MAD/SD value ignores the highly erroneous H2-C7 value. Including H2-C7 gives MAD/SD of 0.42/1.14Hz (see main text and Table S3 for details).

[f] Data reported for lineshape analysis of PIP-HSQMBC for strychnine only.

[g] MAD/SD for PIP-HSQMBC analysis were calculated from only 6 values.

[h] Average $^{n}J_{CH}$ for strychnine found in literature.[4,15,52]

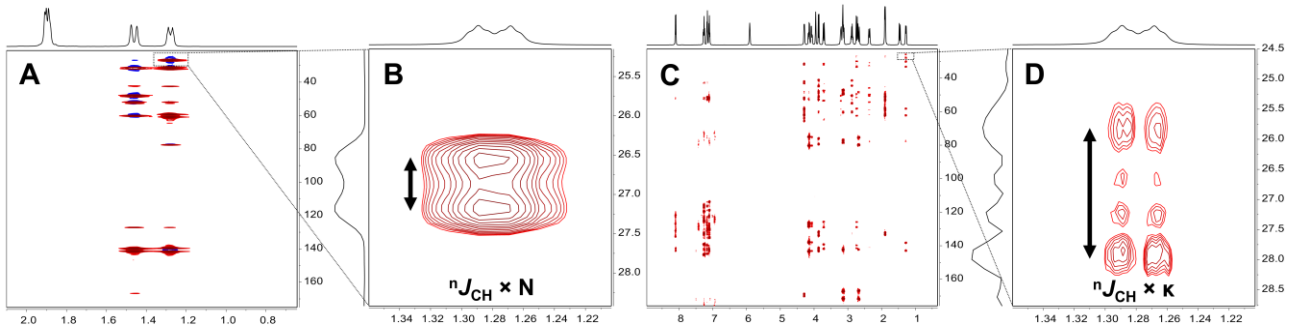

FIGURE 6. F1 measurement of $^nJ_{CH}$ in strychnine A) EXSIDE spectrum for H13 and H15a with J_{LR}=6Hz and N=30, B) *J*-scaled F1 doublet (splitting=77.8Hz) for H13-C15, from which the corresponding $^nJ_{CH}$ (2.6Hz) is measured, C) *J*-HMBC spectrum with J_{LR}=1Hz and κ=79, D) *J*-scaled F1 doublet (splitting=264.3Hz) for H13-C15, from which the corresponding $^nJ_{CH}$ (3.3Hz) is measured.

numbers of t1 increments (typically >10,000 are required for sub-1Hz digital resolution). To circumvent this, it is necessary to use *J*-scaling approaches, which have been reported in both HMBC[20] and HSQMBC-based[19] approaches for model systems where the methods are shown to allow the measurement of even small $^nJ_{CH}$ values. The downside of the longer *J*-scaled evolution periods (typically 200-500ms) is sensitivity losses due to relaxation during these periods. Both HMBC and HSQMBC methods have been reported using such approaches. Herein we use the EXSIDE method (essentially a ^{1}H-selective F1-*J*-scaled HSQMBC) and *J*-HMBC as exemplars.

EXSIDE – Figure 6A shows the EXSIDE spectrum for H13 and H15a of strychnine with correlations between the ^{1}H and each ^{13}C split into simple doublets in the indirect F1 dimension. The $^nJ_{CH}$ value for each ^{1}H-^{13}C pair is readily extracted by dividing the splitting by a user-chosen *J*-scaling factor, N.

The pulse sequence starts with a ^{1}H selective INEPT using a DPFGSE (Double Pulsed Field Gradient Spin Echo) which includes two delay periods of (Δ+τ)/2.[19] The length of τ determines the size of the previously mentioned scaling factor, N, and is a function of t1, τ = N×t1 (typically τ ranges from 200 to 500ms). The user's choice of N is a balance of two main factors; a larger N reduces the t1 data points required to obtain a given resolution in the measured coupling constant, which therefore shortens experiment times. However larger N increases the INEPT delay period for magnetisation transfer and hence nuclei experience more relaxation, which can substantially reduce signal intensity. The length of the INEPT evolution delay Δ is chosen by considering the typical frequency of long range $^nJ_{CH}$ such that Δ=1/(2×$J_{Long\ Range}$), therefore leading to maximum efficiency in the polarisation transfer. The choice of selective ^{1}H inversion pulse and bandwidth can also be crucial where ^{1}H resonances are closely overlapped in the spectrum, however as a general rule a smoothed Gaussian refocussing pulse performed most reliably for 40-90Hz bandwidths, RSnob for 90-250Hz or Reburp for >250Hz while pulses selecting <40Hz bandwidths become too long to practically incorporate into the INEPT period.

Selected $^nJ_{CH}$ data obtained from EXSIDE for strychnine and camphor are presented in Table S3I. The $^nJ_{CH}$ values measured are inherently limited to those arising from protons that could be selectively excited, without exciting one of their ^{1}H-^{1}H

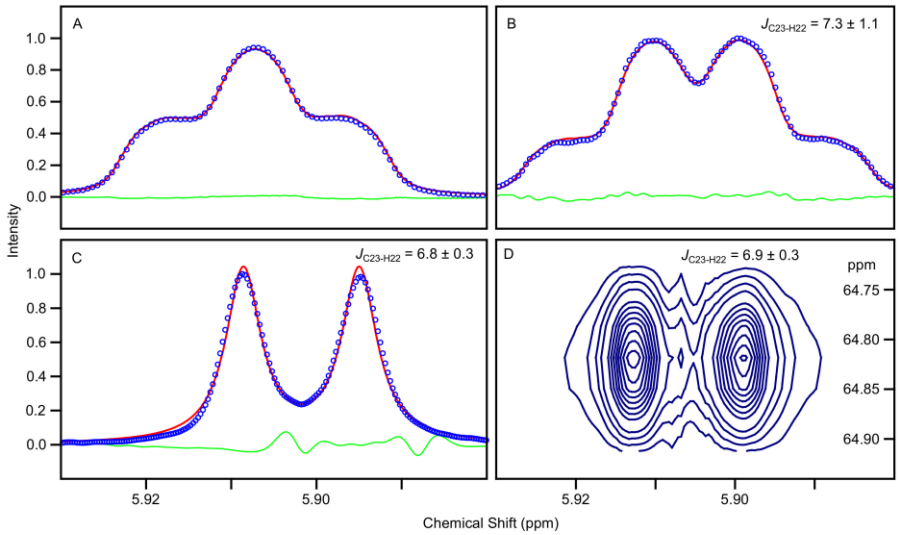

FIGURE 7. Coupling of H22 to C23. A) ^{1}H spectrum. B) PIP-HSQMBC trace (J_{LR}=8Hz), showing the extra coupling to C23 C) HOBS-HSQMBC trace (J_{LR}=8Hz) D) carbon selective HOBS-HSQMBC (J_{LR}=8Hz). Blue circles represent a subset of measured data points. The red line is the result of spectral fitting and the green line is the absolute error.

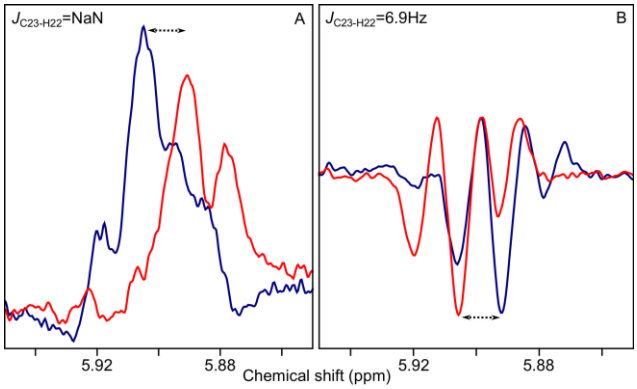

FIGURE 8. H22-C23, strychnine, J_{LR}=8Hz A) refocused HSQMBC B) IPAP HMBC. Blue line represents the sum and the red line is the difference of IP and AP spectra.

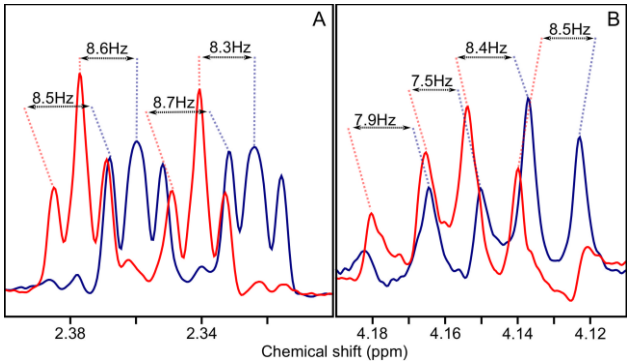

FIGURE 9. Showing the spread of coupling values in sum (red) and difference (blue) for PIP-HSQMBC. A) H1a-C3 of camphor, (J_{LR}=6Hz) B) H23b-C21 of strychnine, (J_{LR}=8Hz).

coupling partners.

***J*-HMBC –** Figure 6C shows the *J*-HMBC spectrum of strychnine with each correlation split in the indirect F1 dimension in the same manner as for EXSIDE, illustrated in Figure 6D for H13-C15, and a similar method for extracting the *J*-scaled $^{n}J_{CH}$ values. The *J*-HMBC pulse sequence[20] achieves *J*-scaling in F1 by incrementing the position of a 180° ^{13}C pulse by κ×t1 within a fixed period of length Δ prior to t1. The scaling factor κ is therefore determined by the F1 spectral width, number of t1 increments and length of Δ. The choice of J_{LR}, which determines Δ(=1/(2×J_{LR})), is set by the size of smallest coupling to be measured rather being set by the size of a typical $^{n}J_{CH}$ value i.e. 6Hz. This gives a typical length of Δ of 500ms or longer. In particular it was found that the lineshape of the correlations in *J*-HMBC were more complex than those arising from the ^{1}H-selective EXSIDE. This can be seen in the expansion of H13-C15 in Figure 6D which is representative of typical lineshapes in these spectra. It was also noted that the lineshape was dependent on the parameters chosen, so changing the scaling factor κ while keeping Δ constant could vary the lineshape quite substantially.

Density Functional Theory Calculations

DFT calculations of $^{n}J_{CH}$ values were also conducted. A total of 101 and 42 $^{n}J_{CH}$ values of >1Hz were obtained for the relatively rigid strychnine and camphor molecules respectively, and those values that can be compared to experimental coupled ^{13}C data are reported in Table S3 for both compounds.

A summary of all of the $^{n}J_{CH}$ data collected in this report is given in Table 1.

Ease of Analysis

Coupled ^{13}C – While experimentally very simple, the coupled ^{13}C spectra were the most demanding spectra to analyse and extract $^{n}J_{CH}$ values from. The resulting spectra generally comprise complex multiplets except in proton sparse molecules, with large $^{1}J_{CH}$ couplings that can introduce additional overlap, hence simulation and lineshape fitting of the entire local ^{1}H and ^{13}C spin system is the only practical solution to extracting accurate $^{n}J_{CH}$ values in most cases. Strychnine and camphor have relatively easily-analysed ^{1}H spin systems but even so only 55 $^{n}J_{CH}$ values could be extracted from coupled ^{13}C spectra out of the 143 estimated by DFT to be >1Hz for these two molecules (Table 1).

Lineshape analysis of PIP-HSQMBC – Similarly, only 20 out of 101 $^{n}J_{CH}$ values for strychnine alone could be extracted from PIP-HSQMBC spectra. Line shape fitting was necessary in order to extract almost any coupling constants at all and accurate fitting of the in-phase lineshapes was often not possible, *i.e.* the fitting was unstable, or Monte Carlo assessment of the fitting errors alone were substantially greater than the desired 0.5Hz accuracy. For example, H22 (Figure 7) shows a very broad apparent triplet ^{1}H resonance, and the H22-C23 PIP-HSQMBC slice shows an ~7Hz coupling, but simulation and fitting of this peak gives a high error range (±1.1Hz) due to uncertainties in the underlying linewidth and multiple small couplings that contribute to the broadened lineshape. In this particular instance the problem can be resolved experimentally because H22 is relatively isolated in the ^{1}H spectrum and thus can be selectively excited and homodecoupled by HOBS-decoupling[50,51] (Figure 7C) with a substantial improvement in the error range for the fitting as well as improved sensitivity. However, in addition to requiring selective excitation, which is not always possible, the HOBS decoupling does artificially broaden the underlying linewidth (to ~2.5Hz in this case), especially where narrow selection bandwidths (and thus long selective pulses) are used, which may make very small couplings hard to measure accurately. Selective excitation also means that generally couplings to only one proton at a time can be measured, so the use of HOBS will substantially increase the required experiment time required if one is interested in measuring all the coupling constants for a molecule by such an approach - hence it is only recommended for resolving challenging multiplets.

IPAP analysis of HSQMBC and HMBC – The IPAP analysis of HSQMBC and HMBC data substantially simplify the extraction of coupling constants by using the offset between the two sum/difference sub-spectra to encode $^{n}J_{CH}$ and do not require lineshape fitting. Where the sum/difference lineshapes are similar, such as shown in Figure 5, then overlaying the spectra and measuring $^{n}J_{CH}$ takes just a few seconds and requires no substantial expert treatment. Even imperfect lineshapes can

be analysed with more confidence in most cases, illustrated in Figure 8B for HMBC (H8-C5 of strychnine) where simple lineshape fitting was not successful, but IPAP allows measurement of the offset between sum (red) and difference (blue) spectra. However in some cases (Figure 8A, H22-C23 of strychnine, refocused HSQMBC) the lineshapes of the sum and difference spectra do not allow any certain extraction of the $^{n}J_{CH}$ value.

This lineshape dependence on accuracy can also be seen in the consistency (or lack of it) when measuring $^{n}J_{CH}$ from the offset between different pairs of lines within the sample multiplet. This is illustrated in Figure 9 for H1a-C3 of camphor and H23b-C21 of strychnine. In the latter case the multiplets can be interpreted as four peaks (which is the correct interpretation) or five (which is not correct - the smallest peak in each multiplet appears to be a sum/difference artefact), so the user must be wary of measurements in distorted lineshapes such as this. It is also clear that the sum/difference lineshapes (red vs blue) are not the same in each case, and so the precise value of $^{n}J_{CH}$ that is measured will depend on which pair of peaks the user selects to measure between, for example in the case of H23b-C21 (strychnine) this leads to a range of ±1.0Hz in the extracted coupling constants depending on the lines selected. In such cases, where we felt a reasonable estimate could be made, the $^{n}J_{CH}$ value we report is the average value of the various measured splittings.

In some cases these difficulties did mean that correlations could not be confidently analysed, but even so IPAP analysis provided the highest number of extracted $^{n}J_{CH}$ values for strychnine and camphor of all the methods studied – 89, 74, and 74 out of 143 for IPAP HMBC, refocused HSQMBC and PIP-HSQMBC respectively, and 96 for IPAP analysis of the accordion HSQMBC.

EXSIDE – The EXSIDE spectrum provides the easiest extraction of $^{n}J_{CH}$ values from a simple F1 doublet (Figure 6A) that reflects $^{n}J_{CH}$ (scaled by a user-defined value, *N*, which is set to 30 in Figure 6A). This extraction from a single spectrum takes only a couple of seconds and provides a powerful argument for employing EXSIDE in a non-expert environment. However, a substantial downside of EXSIDE is that the band-selective ^{1}H pulse cannot include two protons that are mutually coupled (as their ^{1}H-^{1}H coupling could not then be refocussed during evolution of the ^{1}H-^{13}C coupling), so EXSIDE is only effective for regions of the ^{1}H spectrum where protons do not mutually couple, *i.e.*, it cannot be applied in congested spectra where two or more ^{1}H resonances overlap and also couple to each other. Typically EXSIDE is therefore applied on isolated ^{1}H resonances, with the practical limits of efficient and clean selective inversion usually requiring that the resonance is at least 50Hz (0.1ppm at 500MHz) from its nearest coupled partner. In real-world cases this is often not possible and overlap in congested regions of the ^{1}H spectrum of complex molecules can make EXSIDE ineffective for measuring couplings to many (or occasionally all) protons of interest. In the case of strychnine and camphor, which have relatively dispersed ^{1}H spectra, we were able to measure a total of 73 out of 143 $^{n}J_{CH}$ values.

***J*-HMBC** – The *J*-HMBC provides a 'broadband' alternative to the EXSIDE spectrum, as couplings can be measured for essentially all of the protons in the molecule in a single spectrum. However this comes at a price – namely from increased distortion of the F1 lineshape, as illustrated in Figure 6D. The 'correct' coupling constant was assumed to be encoded in the splitting between the largest two peaks in the F1 projection of the corresponding correlation, however substantial secondary bands within the correlation were often as essentially as large as the 'correct' peaks (in this study it was found that the outer bands always corresponded to an appropriate $^{n}J_{CH}$ value with the exception H2-C7 for camphor (see 'Accuracy' section for more details).

Experiment/Analysis Efficiency

Coupled ^{13}C – Because of the direct ^{13}C-detection and complex lineshapes, the coupled ^{13}C spectra take substantial amounts of time to acquire - measurement here entailed concentrated samples (>100mM) combined with a 500MHz ^{13}C-observe cryogenically cooled NMR probe and even so required around 2 hours of acquisition per decoupled or 1 hour per selectively decoupled experiment (of which more than 20 were needed to extract all of the measured values). This led to an average 30 minutes of experiment time per $^{n}J_{CH}$ value extracted from these spectra. The data processing for this fitting was also very time-consuming, taking between 0.5-8 person hours and up to 72 hours of CPU time to fit each peak.

Lineshape analysis of PIP-HSQMBC – PIP-HSQMBC on the other hand is the fastest experimental method, requiring only the acquisition of a single 2D experiment, with the experiment time limited only by sensitivity and the need for digital resolution in the indirect ^{13}C dimension. Consequently when sample quantities are not limiting these experiments take ~1-4 hours per sample depending on the required F1 resolution. Unfortunately the complexity of the lineshapes and necessity for lineshape simulation/fitting to process the data offsets this time advantage quite substantially. Indeed, the challenge of fitting the lineshapes was such that for strychnine only 20 out of 101 $^{n}J_{CH}$ values could be reliably extracted from this experiment (~14 minutes of experiment time per $^{n}J_{CH}$ measured). This is not to say that more values could not be extracted from the more complex peaks, but the fitting procedures became unstable when applied to these and we did not have confidence in the reliability or accuracy of the resulting values. This was exacerbated by the substantial data processing demands of the simulation and fitting of each peak (with concomitant requirement to model the entire local spin system) typically requiring 15-25 minutes to complete.

IPAP analysis of HSQMBC and HMBC – Both IPAP approaches require only two experimental datasets and otherwise are limited only by sensitivity and the need for digital resolution in the indirect ^{13}C dimension. With the experimental conditions and abundant sample cases (>100mM) reported here the experiments took ~3-7 hours to collect both IP/AP datasets giving ~3-6 minutes per $^{n}J_{CH}$ value measured. The ease of data interpretation of the IPAP approach makes this method very efficient for extracting the $^{n}J_{CH}$ values, just a few seconds per

$^{n}J_{CH}$ value in cases such as that shown in Figure 8B. However, for less consistent correlations such as in Figure 8A it was not always immediately obvious how to measure $^{n}J_{CH}$ from the overlaid multiplets, which can slow the process down (and prevent extraction of $^{n}J_{CH}$ in some cases as discussed above).

As noted above, small $^{n}J_{CH}$ values (<2Hz) become difficult to measure due to insensitivity and heavy homonuclear lineshape modulation. This is best illustrated by the number of $^{n}J_{CH}$ values of <1Hz which can be measured by each technique (Table S3). Of the 11 <1Hz $^{n}J_{CH}$ values which could be extracted from coupled ^{13}C spectra, only refocussed HSQMBC and J-HMBC gave any values at all (3 each). HSQMBC-COSY and HMBC-COSY[32] have been proposed to offer more sensitivity to these smallest couplings and indeed did each show 5 couplings of <1Hz – but appear to show slightly fewer larger couplings, so the value in these COSY-style methods is likely to be study-dependant.

EXSIDE – The ^{1}H-selective EXSIDE is experimentally extremely time-inefficient because measurements of $^{n}J_{CH}$ require a separate 2-4 hour EXSIDE spectrum for each ^{1}H (or group of ^{1}H) examined, measured with high digital resolution (500-1500 t1 increments for a full ^{13}C spectrum width, with a *J*-scaling factor of 30). Consequently, experiment time per $^{n}J_{CH}$ value for EXSIDE was ~40 minutes, although where sample quantity is not limiting this can be reduced by an order of magnitude by using F1-band selection[52,53] or non-uniform sampling of the F1 dimension. Finally, as described below, if the most accurate values for $^{n}J_{CH}$ are to be extracted then EXSIDE spectra must be run with multiple INEPT transfer delays (at least four in our experience), necessitating a concomitant 4-fold increase in experimental time, although this can be mostly avoided by applying a correction to the measured $^{n}J_{CH}$ values, *vide infra*.

***J*-HMBC –** The need to run only a single spectrum and the large number of $^{n}J_{CH}$ values which can be extracted make the *J*-HMBC the most experimentally efficient method examined herein (2 minutes of experiment time per $^{n}J_{CH}$ value), but this is substantially offset when extracting each value from the more complex F1 lineshapes arising in these data is substantially more challenging than from EXSIDE. It should also be noted that in some cases, no correlations at all were observed for a given ^{1}H, for example H22 and H15a of strychnine can be clearly seen to give no peaks in the *J*-HMBC (Figure 6C) but do so for the other techniques outlined here. While it is tempting to simply ascribe this insensitivity to relaxation there is no correlation to the measured T1/T2 values for these protons.

Accuracy

Coupled ^{13}C – When multiplets can be fitted, the coupled ^{13}C spectra in principle provide reliably accurate $^{n}J_{CH}$ values, as errors arise only from the quality of fitting the complex in-phase multiplets such as those in Figure 2. The reliability of the lineshape fitting was assessed by comparison of $^{n}J_{CH}$ values obtained from fitting the fully coupled ^{13}C multiplets against those obtained from fitting much simpler selectively-decoupled multiplets (Table S3B), where inaccuracy in the ^{1}H-^{1}H values used to simulate complex multiplets was eliminated. The values obtained from both of these approaches deviated from each other by less than 0.3Hz in all cases, indicating that these values are very reliable indeed. Therefore in the remaining discussion, the coupled ^{13}C data is assumed to provide the most accurate $^{n}J_{CH}$ values available and the accuracy of all subsequent methods will be assessed by comparison to them.

DFT and Literature – Comparison of DFT calculated $^{n}J_{CH}$ values to those obtained by coupled ^{13}C experiments demonstrated that DFT systematically underestimates $^{n}J_{CH}$ by ~6% (Figure S9). This is in line with previous findings for $^{1}J_{CH}$[54] and is ascribed to the fact that DFT calculations are effectively carried out at zero Kelvin (no vibration is accounted for). A systematic 6% increase in DFT-calculated $^{n}J_{CH}$ values is therefore applied herein as a zero-point correction, prior to comparison with experimental data. Comparison of the zero-point corrected DFT $^{n}J_{CH}$ values to the coupled ^{13}C values in this report gave reasonable correlations but with still relatively large mean absolute deviations (MAD, 0.38Hz) and standard deviations (SD, 0.49Hz) from the experimental values. This suggests that there is room for improvement in computational methods in order to match the quality of data able to be derived from experimental methods for moderately complex organic molecules and we hope that this report will enable more robust methods to be tested in future.

For the purposes of comparison, it is also useful to highlight the accuracy of $^{n}J_{CH}$ data from literature sources. Table S3L contains $^{n}J_{CH}$ coupling constants for strychnine found in historical reports[4,15,52,55] using a range of techniques (see SI for details) and we find that the reliability of these values was relatively low when they were compared to the coupled ^{13}C data reported in Table S3B. The MAD of the literature data compared to coupled ^{13}C was 1.04Hz (SD 1.78Hz) although this was dominated by anomalous values included from Blechta *et al.*[55] Removing these values reduced this to 0.62Hz MAD and 0.84Hz SD, which is still rather larger than was found for the recommended methods discussed below.

Lineshape analysis of PIP-HSQMBC – When they could be fitted, the $^{n}J_{CH}$ values extracted from IP PIP-HSQMBC gave surprisingly accurate results (0.18Hz MAD, 0.14Hz SD) in comparison to the values established from coupled ^{13}C spectra. While this suggests that reliable values extracted by this method are highly accurate, it should be noted that these MAD/SD values were calculated from only the 6 couplings that could be measured by *both* IP PIP-HSMQBC and coupled ^{13}C.

IPAP analysis of HSQMBC and HMBC – The variability of lineshape between sum and difference spectra, as illustrated in Figures 4 and 5, is the greatest practical drawback for IPAP-based methods. This prevents the reliable measurement of some $^{n}J_{CH}$ values in some cases (for the purposes of this report, we did not measure $^{n}J_{CH}$ values for the most heavily distorted lineshapes). However, when the sum and difference sub-spectra give comparable lineshapes, IPAP analysis gives good agreement with coupled ^{13}C data (0.35Hz MAD, 0.40Hz SD for HMBC; 0.33Hz MAD, 0.53Hz SD for refocused HSQMBC; 0.22Hz MAD, 0.34Hz SD for PIP-HSQMBC) reflecting the difficulty of accurately assessing coupling constants from some peaks in F2-coupled datasets. In particular, the variability of the $^{n}J_{CH}$

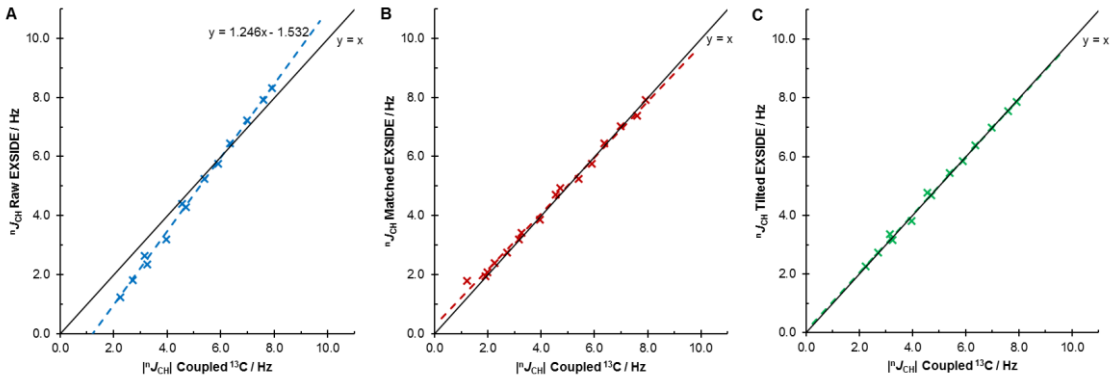

FIGURE 10. Strychnine A) EXSIDE (J_{LR}=6Hz) $^nJ_{HC}$ values *vs* coupled ^{13}C B) $^nJ_{HC}$ values obtained with 'Matching' technique for EXSIDE *vs* coupled ^{13}C C) scaled EXSIDE (J_{LR}=6Hz) $^nJ_{HC}$ values [corrected by $^nJ_{CH}$(scaled) = ($^nJ_{CH}$(EXSIDE, J_{LR}=6Hz) + 1.619) / 1.263)].

values when measured from different peaks of the overlaid multiplets (Figure 5) is a substantial source of any inaccuracy in this method - this can be minimised by calculating $^nJ_{CH}$ as the average of all splittings measured between the sum/difference multiplets. These findings are in line with those reported recently by Pierens *et al*[6] who found average deviations between coupled ^{13}C and IPAP analysis of refocused HSQMBC data of up to 0.2Hz.

EXSIDE – The deviation between EXSIDE $^nJ_{HC}$ values and those obtained from the corresponding coupled ^{13}C spectra for strychnine (Figure 10A, J_{LR}=6Hz) gave a MAD/SD of 0.46Hz/0.48Hz. This deviation is the highest of all the methods examined here and given that the typical range of absolute $^nJ_{CH}$ values is 0-10Hz it might suggest that EXSIDE is only marginally accurate for the assessment of $^nJ_{CH}$ values. However when the EXSIDE experimental data is plotted against the coupled ^{13}C data (Figure 10A) it is clear that there is a systematic variation in the measured $^nJ_{CH}$ values. This arises from a mismatch between the actual $^nJ_{CH}$ value for a given correlation and the chosen INEPT delay period $\Delta=1/(2\times J_{LR})$ of the experiment, causing $^nJ_{HC}$ values smaller than J_{LR} to be underestimated and $^nJ_{HC}$ values larger than J_{LR} to be overestimated. This is illustrated as a function of J_{LR} in Figure 11 where the separation between the peaks of the F1 doublet apparently increases as J_{LR} decreases.

For optimal accuracy, J_{LR} should therefore be equal to $^nJ_{CH}$, but this necessitates the recording of multiple experimental EXSIDE spectra with a range of J_{LR} values. This was tested here with a range of different J_{LR} (10, 8, 6, 4 and 2Hz) and the experimental $^nJ_{CH}$ value was taken to be that measured from the EXSIDE spectrum with the most closely matched J_{LR}. These 'matched' EXSIDE $^nJ_{CH}$ values (Figure 10B) showed much improved agreement with coupled ^{13}C (MAD=0.14Hz, SD=0.19Hz), however this comes at a substantial cost in experiment time as 5-times the number of (already very long) EXSIDE spectra must be obtained. A more rapid alternative to treating the $^nJ_{CH}/J_{LR}$ mismatch is to scale the experimental EXSIDE data based on the trend observed in Figure 10A. This is demonstrated here by using the line of best fit for data from the EXSIDE spectra (J_{LR}=6Hz) for camphor (27 $^nJ_{CH}$ values, slope=1.263, intercept=-1.619) to adjust the corresponding strychnine EXSIDE (J_{LR}=6Hz) data as per Equation 1:

$$^nJ_{CH}(\text{tilted})=(^nJ_{CH}(\text{EXSIDE } J_{LR}=6\text{Hz}) + 1.619) / 1.263) \quad (1)$$

The resulting 'tilted' EXSIDE $^nJ_{CH}$ values for strychnine are shown in Figure 10C and give substantially improved fit to the coupled ^{13}C data (MAD=0.08Hz, SD=0.11Hz), which is even slightly more accurate than was achieved with the matched EXSIDE. It is suggested that tilted EXSIDE data will provide the most time-efficient EXSIDE-based access to accurate $^nJ_{CH}$ values and EXSIDE data acquired with J_{LR}=6Hz should be tilted *via* Equation 2 (derived from fitting of all the strychnine and camphor coupled ^{13}C data to EXSIDE (J_{LR}=6Hz) (73 $^nJ_{CH}$ values, slope=1.256, intercept=1.580, Figure S7I).

$$^nJ_{CH}(\text{scaled}) = (^nJ_{CH}(\text{EXSIDE } J_{LR}=6\text{Hz}) + 1.580) / 1.256) \quad (2)$$

***J*-HMBC –** The large majority of $^nJ_{CH}$ values measured by *J*-HMBC were found to be reasonably accurate (MAD/SD of 0.28Hz/0.44Hz), however this accuracy comes with a significant caveat. As noted above, the substantial lineshape distortion shown in Figure 6D complicates the process of identifying the 'correct' peaks from which to measure the requisite coupling constant. When studying a completely new molecule, this lack of clarity in how to extract $^nJ_{CH}$ from a given correlation makes it difficult to be confident in any one result.

As an example, the MAD/SD reported above excludes the substantially erroneous $^nJ_{CH}$ value corresponding to H2-C7 of camphor (1.0Hz by *J*-HMBC, 8.4-8.7Hz by DFT and all other

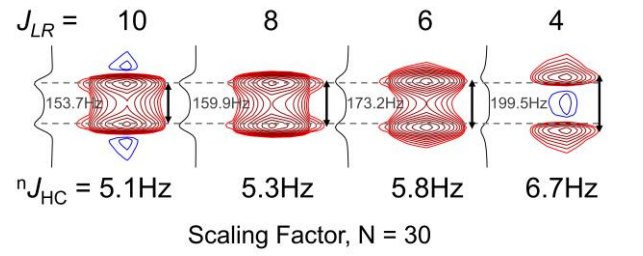

FIGURE 11. $^nJ_{HC}$ values for strychnine, H22-C20, measured with decreasing values of J_{LR}.

experimental methods reported herein, Table S3). The corresponding correlation can be seen in Figure S13 where the EXSIDE (*J*-scaling *N*=30) shows the expected splitting while *J*-HMBC (*J*-scaling κ=78) has no split of the expected scale, instead it suggesting a misleadingly small value. This erroneous value was also observed in the corresponding constant-time variant of the *J*-HMBC[20]. Changing the *J*-scaling factor κ to 30 was observed to mostly restore the lineshape to one which more closely reflected the expected $^{n}J_{CH}$ value (7.5Hz). This dependence of the extractable coupling constant on the parameterisation of the experiment raises significant concerns over the reliability and confidence which can be placed on values extracted from *J*-HMBC. There is no doubt that the large majority of values are accurate, but it is impossible to be certain *a priori* if any given measured value is correct.

Summary

In summary, the accurate measurement of 55 $^{n}J_{CH}$ couplings from coupled ^{13}C spectra has allowed us to assess the ease, efficiency and accuracy of recent F2- and F1- based 2-dimensional methods for measuring $^{n}J_{CH}$ in well-behaved model compounds such as strychnine and camphor. For these compounds, where chemical exchange, line broadening/relaxation and spectrum overlap are not limiting, methods based on full spin-system simulation and/or F2 line-shape fitting (coupled ^{13}C, HSQMBC) are still found to be extremely time intensive for analysis and do not allow the accurate recovery of a large percentage of possible $^{n}J_{CH}$ values. The IPAP-based analysis of HSQMBC and HMBC data were found to be much more robust and efficient, providing the largest number of the expected $^{n}J_{CH}$ values in a relatively short amount of experimental and analysis time. IPAP-based methods also allowed measurement of $^{n}J_{CH}$ with good accuracy (mean deviations of <0.5Hz from coupled ^{13}C data) however care must be taken when extracting $^{n}J_{CH}$ values from heavily distorted lineshapes. The ^{1}H-selective homonuclear decoupled *J*-scaled F1 evolution of $^{n}J_{CH}$ in experiments such as EXSIDE provides the simplest spectra for readout of $^{n}J_{CH}$ but are extremely experimentally time-consuming when couplings for multiple protons are required in the same study. The accuracy of raw EXSIDE-based methods is relatively low due to mismatches between the fixed evolution delay and the range of $^{n}J_{CH}$ values, but this can be substantially improved by the simple data-tilting outlined in Equation 2 and this 'tilted' EXSIDE approach provided the most accurate $^{n}J_{CH}$ data from a 2D-experiment in this report. The much less experimentally time-consuming *J*-HMBC, which also employs F1 *J*-scaling, provides rapid access to $^{n}J_{CH}$ values however the complex lineshapes make confident extraction of accurate values substantially more challenging and in one case we found that an entirely erroneous $^{n}J_{CH}$ value was encoded in the F1 splitting of the corresponding correlation.

Consequently where reliable and accurate extraction of $^{n}J_{CH}$ values is required, we recommend IPAP-based methods for the routine global analysis in larger studies and tilted EXSIDE analysis in non-expert environments or where particularly high accuracy are required.

Acknowledgements

The authors would like to thank Martin J. Watson (C4X Discovery) for helpful conversations and critical review of the manuscript as well as C4X Discovery and University of Bristol's EPSRC Doctoral Training Grant for funding for CD.

Notes and references

[1] A. A. van Beuzekom, F. A. A. M. de Leeuw and C. Altona, *Magn. Reson. Chem.*, 1990, **28**, 68–74.
[2] G. Palermo, R. Riccio and G. Bifulco, *J. Org. Chem.*, 2010, **75**, 1982–1991.
[3] T. Parella and J. F. Espinosa, *Prog. Nucl. Magn. Reson. Spectrosc.*, 2013, **73**, 17–55.
[4] B. L. Marquez, W. H. Gerwick and R. Thomas Williamson, *Magn. Reson. Chem.*, 2001, **39**, 499–530.
[5] L. Castañar, & T. Parella, *Annu. Rep. NMR Spectro.*, 2015, **84**, 163–232.
[6] During the late stages of manuscript preparation, Pierens *et al* reported on the accuracy of $^{n}J_{CH}$ values for cinnamic acids derived from coupled ^{13}C and HSQMBC spectra, and compared these to DFT-derived values: G. K. Pierens, T. K. Venkatachalam and D. C. Reutens, *Magn. Reson. Chem.*, 2016.
[7] L. Castañar, P. Nolis, A. Virgili and T. Parella, *Chem. Eur. J.*, 2013, **19**, 17283–17286.
[8] J. Ying, J. Roche and A. Bax, *J. Magn. Reson.*, 2014, **241**, 97–102.
[9] S. Glanzer and K. Zangger, *J. Am. Chem. Soc.*, 2015, **137**, 5163–5169.
[10] M. Kurz, P. Schmieder and H. Kessler, *Angew. Chem. Int. Ed. Eng.*, 1991, **30**, 1329–1331.
[11] W. Koźmiński and D. Nanz, *J. Magn. Reson.*, 1997, **124**, 383–392.
[12] P. Nolis and T. Parella, *J. Magn. Reson.*, 2005, **176**, 15–26.
[13] W. Koźmiński, *J. Magn. Reson.*, 1999, **137**, 408–412.
[14] J. Stonehouse and J. Keeler, *J. Magn. Reson. Ser. A*, 1995, **112**, 43–57.
[15] R. A. E. Edden and J. Keeler, *J. Magn. Reson.*, 2004, **166**, 53–68.
[16] S. Gil, J. F. Espinosa and T. Parella, *J. Magn. Reson.*, 2010, **207**, 312–321.
[17] S. Gil, J. F. Espinosa and T. Parella, *J. Magn. Reson.*, 2011, **213**, 145–150.
[18] L. Castañar, J. Saurí, R. T. Williamson, A. Virgili and T. Parella, *Angew. Chem. Int. Ed. Engl.*, 2014, **53**, 8379–8382.
[19] V. V Krishnamurthy, *J. Magn. Reson. Ser. A*, 1996, **121**, 33–41.
[20] Meissner, A., Sørensen, O. W., 2001, *Mag. Res. Chem.*, **39**, 49–52.
[21] K. Furihata, M. Tashiro and H. Seto, *Magn. Reson. Chem.*, 2010, **48**, 179–183.
[22] J. Saurí, J. F. Espinosa and T. Parella, *Angew. Chem. Int. Ed. Engl.*, 2012, **51**, 3919–3922.
[23] J. Saurí and T. Parella, *Magn. Reson. Chem.*, 2012, **50**, 717–721.
[24] M. Foroozandeh, R. W. Adams, N. J. Meharry, D. Jeannerat, M. Nilsson and G. A. Morris, *Angew. Chem. Int. Ed..*, 2014, **53**, 6990–6992.
[25] K. Zangger and H. Sterk, *J. Magn. Reson.*, 1997, **124**, 486–489.

[26] M. Mobli and J. C. Hoch, *Prog. Nucl. Magn. Reson. Spectrosc.*, 2014, **83**, 21–41.
[27] M. H. Levitt, R. Freeman and T. Frenkiel, *J. Magn. Reson.*, 1982, **47**, 328–330.
[28] E. Kupce, J. Boyd and I. D. Campbell, *J. Magn. Reson. Ser. B*, 1995, **106**, 300–303.
[29] M. J. Thrippleton and J. Keeler, *Angew. Chem.*, 2003, **115**, 4068–4071.
[30] S. Wimperis and R. Freeman, *J. Magn. Reson.*, 1984, **58**, 348–353.
[31] C. Emetarom, T. L. Hwang, G. Mackin and A. J. Shaka, *J. Magn. Reson. Ser. A*, 1995, **115**, 137–140.
[32] J. Saurí and T. Parella, *Magn. Reson. Chem.*, 2013, **51**, 509–516.
[33] K. Zangger and I. M. Armitage, *Magn. Reson. Chem.*, 2000, **38**, 452–458.
[34] C. E. Hadden and D. T. Angwin, *Magn. Reson. Chem.*, 2001, **39**, 1–8.
[35] F. Delaglio, S. Grzesiek, G. W. Vuister, G. Zhu, J. Pfeifer and A. Bax, *J. Biomol. NMR*, 1995, **6**, 277–293.
[36] Diehl, P.; Kellerhals, H.; Lustig, E. *Computer Assistance in the Analysis of High-Resolution NMR Spectra*. In NMR Basic Principles and Progress; Springer Berlin Heidelberg: Berlin, Heidelberg, 1972; Vol 6.
[37] S. A. Smith, T. O. Levante, B. H. Meier and R. R. Ernst, *J. Magn. Reson. Ser. A*, 1994, **106**, 75–105.
[38] M. Hatlo, F. James, P. Mato, L. Moneta, M. Winkler and A. Zsenei, *IEEE Trans. Nucl. Sci.*, 2005, **52**, 2818–2822.
[39] J. A. Nelder and R. Mead, *Comput. J.* , 1965, **7**, 308–313.
[40] X. Han, V. Pozdina, C. Haridas and P. Misra, *J. Inf. Comput. Sci.*, 2006.
[41] Gaussian 09, Revision D.01, Frisch, M. J.; Trucks, G. W.; Schlegel, H. B.; Scuseria, G. E.; Robb, M. A.; Cheeseman, J. R.; Scalmani, G.; Barone, V.; Mennucci, B.; Petersson, G. A.; Nakatsuji, H.; Caricato, M.; Li, X.; Hratchian, H. P.; Izmaylov, A. F.; Bloino, J.; Zheng, G.; Sonnenberg, J. L.; Hada, M.; Ehara, M.; Toyota, K.; Fukuda, R.; Hasegawa, J.; Ishida, M.; Nakajima, T.; Honda, Y.; Kitao, O.; Nakai, H.; Vreven, T.; Montgomery, J. A., Jr.; Peralta, J. E.; Ogliaro, F.; Bearpark, M.; Heyd, J. J.; Brothers, E.; Kudin, K. N.; Staroverov, V. N.; Kobayashi, R.; Normand, J.; Raghavachari, K.; Rendell, A.; Burant, J. C.; Iyengar, S. S.; Tomasi, J.; Cossi, M.; Rega, N.; Millam, J. M.; Klene, M.; Knox, J. E.; Cross, J. B.; Bakken, V.; Adamo, C.; Jaramillo, J.; Gomperts, R.; Stratmann, R. E.; Yazyev, O.; Austin, A. J.; Cammi, R.; Pomelli, C.; Ochterski, J. W.; Martin, R. L.; Morokuma, K.; Zakrzewski, V. G.; Voth, G. A.; Salvador, P.; Dannenberg, J. J.; Dapprich, S.; Daniels, A. D.; Farkas, Ö.; Foresman, J. B.; Ortiz, J. V.; Cioslowski, J.; Fox, D. J. Gaussian, Inc., Wallingford CT, 2013.
[42] A. W. Douglas and M. Shapiro, *Org. Magn. Reson.*, 1980, **14**, 38–39.
[43] A. Meissner, J. Ø. Duus and O. W. Sørensen, *J. Biomol. NMR*, 1997, **10**, 89–94.
[44] M. Ottiger, F. Delaglio and A. Bax, *J. Magn. Reson.*, 1998, **131**, 373–378.
[45] R. T. Williamson, B. L. Marquez, W. H. Gerwick and K. E. Kövér, *Magn. Reson. Chem.*, 2000, **38**, 265–273.
[46] S. Boros and K. E. Kövér, *Magn. Reson. Chem.*, 2011, **49**, 106–110.
[47] I. Timári, L. Szilágyi and K. E. Kövér, *Chem. Eur. J.*, 2015, **21**, 13939–13942.
[48] J. Sauri, T. Parella and J. F. Espinosa, *Org. Biomol. Chem.*, 2013, **11**, 4473–4478.
[49] A. Bax, K.A. Farley, G.S. Walker, , *J. Magn. Reson. Ser. A*, 1996 **119** 134–138.
[50] L. Castañar, J. Saurí, P. Nolis, A. Virgili and T. Parella, *J. Magn. Reson.*, 2014, **238**, 63–69.
[51] L. Castañar, R. Roldán, P. Clapés, A. Virgili and T. Parella, *Chem. Eur. J*, 2015, **21**, 7682–7685.
[52] C. P. Butts, B. Heise and G. Tatolo, *Org. Lett.*, 2012, **14**, 3256–3259.
[53] I. E. Ndukwe and C. P. Butts, *RSC Adv.*, 2015, **5**, 107829–107832.
[54] J. San Fabián, J. M. García de la Vega, R. Suardíaz, M. Fernández-Oliva, C. Pérez, R. Crespo-Otero and R. H. Contreras, *Magn. Reson. Chem.*, 2013, **51**, 775–787.
[55] V. Blechta, F. del Río-Portilla and R. Freeman, *Magn. Reson. Chem.*, 1994, **32**, 134–137.